Polydopamine-Inspired, Dual Heteroatom-Doped Carbon Nanotubes for Highly Efficient Overall Water Splitting

Konggang Qu, Yao Zheng, Yan Jiao, Xianxi Zhang, Sheng Dai and Shi-Zhang Qiao**

Dr. Konggang Qu, Yao Zheng, Yan Jiao, Prof. Sheng Dai, Prof. Shi-Zhang Qiao
School of Chemical Engineering, The University of Adelaide, Adelaide, SA 5005, Australia
E-mail: s.dai@adelaide.edu.au; s.qiao@adelaide.edu.au

Dr. Konggang Qu, Prof. Xianxi Zhang
Shandong Provincial Key Laboratory of Chemical Energy Storage and Novel Cell Technology, School of Chemistry and Chemical Engineering, Liaocheng University, Liaocheng 252059, China

Prof. Shi-Zhang Qiao
School of Materials Science and Engineering, Tianjin University, Tianjin 300072, China.

Dr. Konggang Qu and Yao Zheng contributed equally to this work.

Keywords: bifunctional electrocatalysts, nonmetallic codoping, carbon nanotube, polydopamine, water splitting

Abstract: Overall water splitting involved hydrogen evolution reaction (HER) and oxygen evolution reaction (OER) is critical to renewable energy conversion and storage. Heteroatom-doped carbon materials have been extensively employed as the efficient electrocatalysts for independent HER or OER process, while those as the bifunctional catalysts for simultaneously generating H_2 and O_2 by splitting water have been yet seldom reported. Inspired by the unparalleled virtues of polydopamine (PDA), we devise the facile synthesis of nitrogen and sulfur dual-doped carbon nanotubes (N,S-CNT) with *in-situ*, homogenous and high concentration sulfur doping. The newly developed dual-doped electrocatalysts display superb bifunctional catalytic activities for both the HER and OER in alkaline solutions, outperforming all other reported carbon counterparts. Experimental characterizations confirm that the excellent performance is attributed to the multiple doping together with efficient mass and charge transfer, while theoretical computations reveal the promotion effect of secondary sulfur dopant to enhance the spin density of dual-doped samples and consequently to form highly electroactive sites for both HER and OER.

1. Introduction

Photoelectrochemical water splitting has triggered huge interest as the promising technology for efficient renewable energy conversion.[1-3] Currently, the most efficient catalysts to split water are noble metals like Pt, Ir, and Ru, *etc.* for cathodic hydrogen evolution reaction (HER)[4-5] and anodic oxygen evolution reaction (OER).[6-7] Extensive efforts have been undertaken toward using earth-abundant metal materials to replace noble metals, such as the transition-metal sulfides,[8-9] phosphides,[10-12] carbides,[13-14] borides[13] for HER and the oxides/hydroxides of Co,[15] Ni,[16] Mn,[17] Fe[18-19] for OER. Practically, to achieve an overall water splitting generating oxygen and hydrogen simultaneously, the coupling of HER and OER catalysts in same electrolyte often results in incompatible integration of the catalysts and leads to inferior overall performance. As a result, CoO_x,[20] $NiFeO_x$,[21] CoP film[22] and NiSe nanowire[23] have been developped as efficiently bifunctinal HER and OER catalysts. However, inherent corrosion and oxidation susceptibility of these materials in either strongly acidic or alkaline solution largely limit their sustainable utilization, which in most cases underperform noble-metal catalysts.

In recent years, non-metallic heteroatom-doped carbon materials have been intensively studied for energy-related electrocatalytic reactions such as oxygen reduction reaction (ORR),[24-26] OER[27-28] and HER[29-32] due to their excellent electrical conductivity, tunable molecular structures, abundance, and strong tolerance to acidic/alkaline environments. Impressively, engineering carbon materials by codoping two or more selected heteroatoms greatly boosts their elctrocatalytic activities through synergistic coupling effect,[31, 33] but more importantly, it can realize tailorable catalytic capabilities for specific electrocatalytic reactions by altering doping types, sites and levels.[34-36] Correspondingly, several carbon materials have been synthesized for the bifunctional ORR and OER electrocatalysts with high activity and excellent stability.[35, 37-38] Although some of these have recently been successfully developed as the HER electrocatalysts,[29-32] the employment of carbon-based

nanomaterials as the bifunctional HER and OER electrocatalysts has not been reported to date. The possible reason is that the ORR and OER performance of carbon materials can be comparable to or even better than metal-based catalysts, but the HER catalytic efficiency of carbon-based materials still falls far short of that of the metallic benchmarks.[39-41] This represents the current bottleneck for the development of bifunctional HER and OER carbon electrocatalysts for overall water splitting.

Recently, we demonstrated the unparalleled virtues of polydopamine (PDA) can be applied as an excellent platform for constructing multiple heteroatom-doped carbon materials for electrocatalytic ORR and OER.[38, 42] In particular, PDA is extremely reactive to thiol groups via Schiff-base or Michael addition reaction at room temperature without any harsh reaction condition.[43] After thiol addition to PDA, it is easily to realize the N,S-codoped carbon materials. Apart from discarding excessive N and S sources which are indispensible for the traditional post-doping method by high temperature annealing,[32, 44] more crucially, this PDA-assisted N,S co-doping strategy can effectively improve the S-doping efficiency arising from the high grafting efficiency of thiol groups.

Guiding by this strategy, herein we report a two-step “graft-and-pyrolyze” route to achieve N, S co-doping carbon materials which is fully different from current post-treatment methods. PDA was first facilely deposited onto the surface of multi-walled carbon nanotubes (CNT) and then chemically grafted with the thiol groups of S-precursors at room temperature (see **Scheme 1**). After pyrolysis at high temperatures, this simple synthetic approach can derive *in situ* and homogeneous N,S-codoping in the carbon framework with higher S-doping efficiency (5.6 at. %) than most of reported methods. As a result, the obtained N,S-CNTs exhibit superior bifunctional OER and HER eletrocatalytic activities in alkaline solutions, better than most of reported carbon electrocatalysts. The combination of experimental characterizations and density functional theory (DFT) calculations jointly unveil the origin of this large activity enhancement. The results show the secondary S-doping plays a critical role

in the formation of catalytically active sites and enhancements of charge transfer. Considering N and S are the most important dopants in carbon materials for electrocatalysis, this promising synthetic method may open a new avenue to the development of carbon-based catalysts for broader applications.[30, 32, 38]

2. Results and Discussion

The morphologies and structures of the as-prepared N,S-CNT were investigated by the transmission electron microscopy (TEM). As expected, the N,S-CNT well maintains its nanotube structure (**Figure 1**A, Figure S1A-B), and the magnified TEM images (Figure 1B, Figure S1C-D) indicate there is the continuous film with a thickness of approximately 2 nm wrapping outside the intrinsic lattice fringe of CNTs, originating from the carbonization of S-modified PDA coating. Typical elemental mapping images of N,S-CNT (Figure 1C-F) illustrate the uniform dispersion of N, O and S elements, also confirming the homogeneous deposition of PDA on CNTs and the following S-addition reaction on PDA. Nitrogen adsorption confirms the N,S-CNT exhibits a large surface area of 149 $m^2 g^{-1}$. The pore size distribution (PSD) curve (Figure S2) further verifies the presence of mesopores with their sizes centered at 3.0 nm and large pores with their sizes ranging from 20 to 150 nm, which are attributable to the inner cavities of the CNT and the voids in the cross-stacking CNT network, respectively.[34]

The characteristic peaks of CNT-PDA at 1501 and 1608 cm^{-1} in the Fourier transform infrared (FTIR) spectra (Figure 1G) are consistent with the indole or indoline structures of PDA,[43] indicating the successful deposition of PDA. For the CNT-PDA modified by sulfur (CPS), the grafting of *2*-mercaptoethanol on the CNT-PDA is evidenced by the weak band at 637 cm^{-1} that corresponds to the C-S bonds.[38] Meanwhile, compared with CNT-PDA, the peak at 1501 cm^{-1} blue shifts to 1509 cm^{-1} and the peak at 1608 cm^{-1} is split into two peaks with a major peak at 1622 cm^{-1} and a shoulder peak at 1588 cm^{-1}. These changes probably

originate from the strong covalent interaction between thiol and PDA. Raman spectra also support the successful introduction of sulfur atoms (Figure 1H). Specifically, the I_D/I_G ratio of N,S-CNT (0.78) is higher than that of N-CNT (0.71), indicating more defects and disordered structures in the N,S-CNT.[45]

The chemical statuses of three elements were evaluated by X-ray photoelectron spectroscopy (XPS) as shown in **Figure 2** and Figure S3. The survey scan illustrates the existence of 3.8 % N and 5.6 % S in N,S-CNT, indicating new preparation method has much higher S-doping efficiency than most of reported methods; a detailed comparison of various S-doping methods is summarized in Table S1. Additionally, the high-resolution N 1s spectra can be deconvoluted into two peaks locating at 398.0 and 400.8 eV, which can be assigned to pyridinic N (p-N) and graphitic N (g-N). The high-resolution S 2p peaks are mainly deconvoluted into three peaks associated with C-S-C (163.2 eV for S $2p_{3/2}$,164.4 eV for S $2p_{1/2}$) and C-SO_x-C (167.8 eV) species. Notably, significant amount of O species (up to 16.5 %) are observed including HO-C=O (530.8 eV), C=O (532.1 eV) and C-OH (533.2 eV), which arise from PDA and can render the electrocatalysts highly hydrophilic for more accessible catalytic surfaces.

The electrocatalytic HER/OER performances for different carbon catalysts were assessed in 1.0 M KOH solutions. For the HER branch shown in **Figure 3**A, the operating potential of N,S-CNT is -0.40 V to deliver a cathodic current density of 5 mA cm^{-2}, much lower than that on CNT-PDA (-0.68 V), oxidized CNT (ox-CNT, -0.61 V) and N-CNT (-0.54 V) control samples, indicating the unique role of S-doping towards electrocatalytic process. Also shown in Figure S4, this potential value has largely outperformed those on previously reported single/dual doped carbon-based materials including N, P-G (-0.58 V),[31] N-G (-0.64 V),[31] S-G (-0.72 V),[31] N-carbon (-0.78 V)[46] and MWCNT (-0.8 V)[47] (The definition of these electrocatalysts can be referred to the caption of Figure S4). It should be noted that the activity of N,S-CNT still has a gap with that of Pt/C, which stands for the benchmark catalyst

for HER (Figure S5A), however, N,S-CNT has a potential decrease of 0.17 V to deliver 5 mA cm^{-2} in comparison with C_3N_4@NG,[30] the best carbon counterpart reported in alkaline solutions, suggesting a dramatic improvement in HER activity. Additionally, N,S-CNT exhibits a Tafel slope value of 133 mV $decade^{-1}$ (Figure 3B), which is also smaller than that of CNT-PDA (178 mV $decade^{-1}$), ox-CNT (165 mV $decade^{-1}$) and N-CNT (187 mV $decade^{-1}$), implying the favorable HER kinetics by dual doping.

On the OER branch, to deliver a 10 mA cm^{-2} current density ($E_{j=10}$) that is a critical metric related to solar fuel production, the operating potential of N,S-CNT is 1.59 V with a small Tafel slope value of 56 mV $decade^{-1}$ (Figures 3C and 3D), which are superior to those of CNT-PDA (1.80 V, 111 mV $decade^{-1}$), ox-CNT (1.66 V, 97 mV $decade^{-1}$) and N-CNT (1.64 V, 87 mV $decade^{-1}$), and also lower than those of reported C_3N_4/CNT (1.60 V, 83 mV $decade^{-1}$)[28], P-C_3N_4 (1.63 V, 61.6 mV $decade^{-1}$)[37], NGSH (1.63 V, 83 mV $decade^{-1}$),[48] MWCNT (1.68 V, 60 mV $decade^{-1}$),[49] CNT@NCNT (1.76 V, not given)[50] and C_3N_4@G (1.78 V, 68.5 mV $decade^{-1}$).[51] It is worth noting that the performance of N,S-CNT is comparable to that of the most active metal-free catalysts reported very recently including echo-MWCNT (1.59 V, 41 mV $decade^{-1}$),[52] S-CNT/G (1.58 V, 95 mV $decade^{-1}$)[53] and N, S-graphite foam (1.576 V, 78 mV $decade^{-1}$),[54] and also the benchmarked IrO_2/CNT (1.59 V, 90 mV $decade^{-1}$)[28] (The definition of various electrocatalysts here can be referred to the caption of Figures S4 and S5).

The stability of gases evolution on N,S-CNT *via* HER and OER processes was investigated by a rotating ring-disk electrode (RRDE) technique. As illustrated on Figure S6, on the HER branch, the generated hydrogen gas on the disk electrode can be directly detected by the ring current that accords with a hydrogen oxidation reaction (HOR) process. Accordingly, oxygen gas can be monitored by the ring current via the ORR process. As shown in Figures 3E and 3F, two ring electrodes display very clear and stable currents in 2000 second (s) testing time, indicating the excellent stability of electrode catalysts and their benign surface property for gas diffusion. This may be assigned to the fact that the robust adhesion of

PDA endows the two-component (CNT and PDA) integrated carbon with the mutually strong coupling and excellent structural stability,[55] which is greatly conducive to the catalytic durability in electrochemical tests.

Given that N,S-CNT is a highly active and stable catalyst toward both HER and OER, we expect the N,S-CNT could act as a bifunctional electrocatalyst for overall water splitting. The as-prepared N,S-CNT was loaded onto the pretreated carbon cloth, which serves as both anode and cathode in a two-electrode configuration (Figure S7A). A catalytic current is observed when the applied potential is larger than 1.90 V (Figure S7B). This alkaline water electrolyzer exhibits effcient performance with the need of a cell voltage of 2.03 V to afford 10 mA cm^{-2} current with vigorous gas evolution on both electrodes. The long-term durability of this system was also evaluated for 20 hour (h) in 1.0 M KOH (Figure S7C). The initial current shows a slow attenuation within 3 h, probably due to slightly peeling off carbon cloth of N,S-CNT during the evolution of H_2 and O_2 gases; afterwards, the current remains unchanged during more than 15 h, confirming the extreme stability of the N,S-CNT in catalyzing overall water splitting.

To reveal the origin of activity enhancement in this co-doped sample, we conducted DFT computations to investigate the promotion effect of the secondary S element doping. According to the XPS characterizations, graphene frameworks doped by N/S atoms at different sites were constructed (Figure S8). It is well known that doping carbon with heteroatoms of different electronegativities can tailor the electron donor-acceptor behaivor and thus improve the apparent catalytic activities of doped samples.[15] However, owing to the nearly identical electronegativity of S (2.58) and C (2.55), the charge transfer between S and C is negligible. Additionally, our computation results show that the chagre density differences around nitogen atoms before and after S doping are highly similar (**Figure 4**A and S9A). These phenomena suggest that such significant activity enhancement caused by the S doping cannot be attributed to the change in electron charge density. Alternatively, previous

theoretical studies on graphene-based materials confirmed that the adsorption strengths of H* and OOH*, which are the key reaction intermediates of HER and OER, respectively, exhibit a correlation with spin density.[56-58] As shown in Figure 4B and S9B, the spin density differences in co-doped models are much more significant than those of single N doped ones. Hence, a larger number of carbon atoms could serve as electrocatalytical active sites to adsorb H* and OOH* reaction intermidates after the secondary S element doping. As a result, the appearent activities (both HER and OER) have been remarkably boosted comparing with single doped ones, as shown in Figure 3.

Besides the unique componential feature, the existing hierarchical pores in the N,S-CNT proved by nitrogen adsorption afford a high electrochemical double layer capacitance (C_{dl}), which is proportional to the active surface areas. As shown in Figure S10, the C_{dl} of N,S-CNT of 4.75 mF cm^{-2} is much higher than that of N-CNT (2.02 mF cm^{-2}) and ox-CNT (1.78 mF cm^{-2}), which makes better exposure and enhanced utilization of the aforementioned active sites on the N,S-CNT, contributing to its efficient HER and OER activities.[35] On the other hand, the existence of abundant pores also facilitates the smooth transportation of reactants and products, and thus expediting the HER and OER catalytic processes.[28] Moreover, the highly conductive CNT and the strong coupling between two components (CNT and PDA) guarantee the favorable charge transfer.[28] Accordingly, the semicircular diameter in the electrochemical impedance spectrum (EIS) of N,S-CNT is much smaller than that of ox-CNT and N-CNT (Figure S11), owing to a smaller contact and charge-transfer impedance. Consequently, the superior bifunctional electrocatalytic performance of N,S-CNT for HER and OER can be attributed to the abundant electroactive sites produced by componentially multiple doping, meanwhile, the structurally hierarchical pores and excellent electrical conductivity assure the smooth electrocatalytic process of active sites.

3. Conclusion

In summary, taking advantage of polydopamine chemistry, we have developed a novel and facile strategy to produce N,S-codoping carbon nanotubes with *in-situ*, homogenous and highly efficient S-doping. The resultant N,S-CNT can be applied as the HER and OER electrocatalysts simultaneously. As far as we are aware, the bifunctional N,S-CNT exhibits the best HER catalytic activity and also is one of the most active OER catalysts, comparing with the previously reported carbon-based HER and OER electrocatalysts. The combination of experimental characterizations and DFT calculations further confirms such excellent activity on N,S-CNT originates from the formation of a large amount of electrocatalytically active sites.

4. Experimental Section

Preparation of N,S-CNT: For the synthesis of N,S-CNT, typically, 85 mL of ox-CNT dispersion (2 mg mL^{-1}) was mixed with 125 mg of dopamine (DA) dissolved in 10 mL of Milli-Q water. The mixture and another 130 ml of Milli-Q water were sonicated for 5 min. Then, 25 mL of PBS buffer (0.4 M, pH=8.5) was added. The mixture was continuously stirred at room temperature for 24 h. After that, 125 mg of 2-mercaptoethanol was added and stirred continually for another 12 h. The CPS hybrids were collected by centrifugation and washed for three times with water. On the other hand, the CNT-PDA hybrids were also prepared according to the same procedure but without the addition of 2-mercaptoethanol.

The N,S-CNT was prepared through the carbonization of CPS hybrids in a temperature-programmable tube furnace under N_2 atmosphere at 400 ^oC for 2 h with a heating rate of 1 ^oC min^{-1}, which was followed by further treatment at 700 ^oC for 3 h with a heating rate of 5 ^oC min^{-1}. For the control experiments, the CNT-PDA hybrids were pyrolyzed under the same condition to obtain the N-CNT.

Electrocatalytic HER and OER Activity Evaluation: For the electrochemical tests, 2 mg of the fabricated catalysts was dispersed in 1 ml of Milli-Q water. The mixture was slightly ultrasonicated to obtain a homogenous catalyst ink. To prepare the working electrode for electrochemical measurements, 20 μl of the ink was dripped on a mirror polished glass carbon electrode. Then, 5 μl of 0.5 wt% Nafion aqueous solution was dripped on the electrode and dried at room temperature as a binder (See supporting information for more details).

Computational Methods: The electron charge density and spin density was computed using DFT with spin-polarization by a VASP code.[59-62] The electronic exchange-correlation was dealt using the Perdew-Burke-Ernzerhof (PBE) functional within the generalized gradient approximation (GGA).[63-64] A 400 eV kinetic energy cut-off was used for the plane-wave expansion. The convergence criterion for electronic structure iteration was set to be 10^{-6} eV and that for geometry optimization was 0.1 eV/Å. A Gaussian smearing of 0.2 eV was applied during the geometry optimization and for the total energy computations, The K-points were set to be 3 × 3 × 1 for graphene sheet-models, and 3 × 1 × 1 for graphene nanoribbon-models.

Supporting Information

Supporting Information is available from the Wiley Online Library or from the author.

Acknowledgements

This work was financially supported by the Australian Research Council (ARC) through Discovery Projects of DP160104866, DP140104062, DP130104459 and DE160101163. The authors also thank the National Natural Science Foundation of China (21601078, 21503104, 21576202), Shandong Province Natural Science Foundation (ZR2014BQ010), and High Education Science and Technology Program of Shandong (J16LC03 and J16LC05) for financial support.

Received: ((will be filled in by the editorial staff))
Revised: ((will be filled in by the editorial staff))
Published online: ((will be filled in by the editorial staff))

[1] J. A. Turner, *Science* **2004**, *305*, 972.

[2] N. S. Lewis, D. G. Nocera, *Proc. Natl. Acad. Sci. USA* **2006**, *103*, 15729.

[3] J. K. Norskov, C. H. Christensen, *Science* **2006**, *312*, 1322.

[4] J. Greeley, T. F. Jaramillo, J. Bonde, I. Chorkendorff, J. K. Norskov, *Nat. Mater.* **2006**, *5*, 909.

[5] R. Subbaraman, D. Tripkovic, D. Strmcnik, K.-C. Chang, M. Uchimura, A. P. Paulikas, V. Stamenkovic, N. M. Markovic, *Science* **2011**, *334*, 1256.

[6] T. Reier, M. Oezaslan, P. Strasser, *ACS Catal.* **2012**, *2*, 1765.

[7] I. Katsounaros, S. Cherevko, A. R. Zeradjanin, K. J. J. Mayrhofer, *Angew. Chem. Int. Ed.* **2014**, *53*, 102.

[8] T. F. Jaramillo, K. P. Jørgensen, J. Bonde, J. H. Nielsen, S. Horch, I. Chorkendorff, *Science* **2007**, *317*, 100.

[9] J. Kibsgaard, Z. Chen, B. N. Reinecke, T. F. Jaramillo, *Nat. Mater.* **2012**, *11*, 963.

[10] Z. Xing, Q. Liu, A. M. Asiri, X. Sun, *Adv. Mater.* **2014**, *26*, 5702.

[11] E. J. Popczun, C. G. Read, C. W. Roske, N. S. Lewis, R. E. Schaak, *Angew. Chem. Int. Ed.* **2014**, *126*, 5531.

[12] P. Jiang, Q. Liu, Y. Liang, J. Tian, A. M. Asiri, X. Sun, *Angew. Chem. Int. Ed.* **2014**, *53*, 12855.

[13] H. Vrubel, X. Hu, *Angew. Chem. Int. Ed.* **2012**, *124*, 12875.

[14] L. Liao, S. Wang, J. Xiao, X. Bian, Y. Zhang, M. D. Scanlon, X. Hu, Y. Tang, B. Liu, H. H. Girault, *Energy Environ. Sci.* **2014**, *7*, 387.

[15] M. W. Kanan, D. G. Nocera, *Science* **2008**, *321*, 1072.

[16] M. Dincă, Y. Surendranath, D. G. Nocera, *Proc. Natl. Acad. Sci. USA* **2010**, *107*, 10337.

[17] F. Song, X. Hu, *J. Am. Chem. Soc.* **2014**, *136*, 16481.

[18] R. D. L. Smith, M. S. Prévot, R. D. Fagan, Z. Zhang, P. A. Sedach, M. K. J. Siu, S. Trudel, C. P. Berlinguette, *Science* **2013**, *340*, 60.

[19] D. Friebel, M. W. Louie, M. Bajdich, K. E. Sanwald, Y. Cai, A. M. Wise, M.-J. Cheng, D. Sokaras, T.-C. Weng, R. Alonso-Mori, R. C. Davis, J. R. Bargar, J. K. Nørskov, A. Nilsson, A. T. Bell, *J. Am. Chem. Soc.* **2015**, *137*, 1305.

[20] H. Jin, J. Wang, D. Su, Z. Wei, Z. Pang, Y. Wang, *J. Am. Chem. Soc.* **2015**, *137*, 2688.

[21] H. Wang, H.-W. Lee, Y. Deng, Z. Lu, P.-C. Hsu, Y. Liu, D. Lin, Y. Cui, *Nat. Commun.* **2015**, *6*, 7261.

[22] N. Jiang, B. You, M. Sheng, Y. Sun, *Angew. Chem. Int. Ed.* **2015**, *54*, 6251.

[23] C. Tang, N. Cheng, Z. Pu, W. Xing, X. Sun, *Angew. Chem. Int. Ed.* **2015**, *54*, 9351.

[24] K. Gong, F. Du, Z. Xia, M. Durstock, L. Dai, *Science* **2009**, *323*, 760.

[25] Y. Zheng, Y. Jiao, J. Chen, J. Liu, J. Liang, A. Du, W. Zhang, Z. Zhu, S. C. Smith, M. Jaroniec, G. Q. Lu, S. Z. Qiao, *J. Am. Chem. Soc.* **2011**, *133*, 20116.

[26] Y. Jiao, Y. Zheng, M. Jaroniec, S. Z. Qiao, *J. Am. Chem. Soc.* **2014**, *136*, 4394.

[27] Y. Zhao, R. Nakamura, K. Kamiya, S. Nakanishi, K. Hashimoto, *Nat. Commun.* **2013**, *4*, 2390.

[28] T. Y. Ma, S. Dai, M. Jaroniec, S. Z. Qiao, *Angew. Chem. Int. Ed.* **2014**, *53*, 7281.

[29] Y. Zhao, F. Zhao, X. Wang, C. Xu, Z. Zhang, G. Shi, L. Qu, *Angew. Chem. Int. Ed.* **2014**, *53*, 13934.

[30] Y. Zheng, Y. Jiao, Y. Zhu, L. H. Li, Y. Han, Y. Chen, A. Du, M. Jaroniec, S. Z. Qiao, *Nat. Commun.* **2014**, *5*, 3783.

[31] Y. Zheng, Y. Jiao, L. H. Li, T. Xing, Y. Chen, M. Jaroniec, S. Z. Qiao, *ACS Nano* **2014**, *8*, 5290.

[32] Y. Ito, W. Cong, T. Fujita, Z. Tang, M. Chen, *Angew. Chem. Int. Ed.* **2015**, *54*, 2131.

[33] J. Liang, Y. Jiao, M. Jaroniec, S. Z. Qiao, *Angew. Chem. Int. Ed.* **2012**, *51*, 11496.

[34] S. Chen, J. Duan, M. Jaroniec, S.-Z. Qiao, *Adv. Mater.* **2014**, *26*, 2925.

[35] J. Zhang, Z. Zhao, Z. Xia, L. Dai, *Nat. Nanotech.* **2015**, *10*, 444.

[36] H. B. Yang, J. Miao, S.-F. Hung, J. Chen, H. B. Tao, X. Wang, L. Zhang, R. Chen, J. Gao, H. M. Chen, L. Dai, B. Liu, *Sci. Adv.* **2016**, *2*, e1501122.

[37] T. Y. Ma, J. Ran, S. Dai, M. Jaroniec, S. Z. Qiao, *Angew. Chem. Int. Ed.* **2015**, *54*, 4646.

[38] K. Qu, Y. Zheng, S. Dai, S. Z. Qiao, *Nano Energy* **2016**, *19*, 373.

[39] Y. Jiao, Y. Zheng, M. Jaroniec, S. Z. Qiao, *Chem. Soc. Rev.* **2015**, *44*, 2060.

[40] Y. Zheng, Y. Jiao, M. Jaroniec, Y. Jin, S. Z. Qiao, *Small* **2012**, *8*, 3550.

[41] Y. Zheng, Y. Jiao, M. Jaroniec, S. Z. Qiao, *Angew. Chem. Int. Ed.* **2015**, *54*, 52.

[42] K. Qu, Y. Zheng, S. Dai, S. Z. Qiao, *Nanoscale* **2015**, *7*, 12598.

[43] H. Lee, S. M. Dellatore, W. M. Miller, P. B. Messersmith, *Science* **2007**, *318*, 426.

[44] S. Yang, L. Zhi, K. Tang, X. Feng, J. Maier, K. Müllen, *Adv. Funct. Mater.* **2012**, *22*, 3634.

[45] Y. Zheng, Y. Jiao, L. Ge, M. Jaroniec, S. Z. Qiao, *Angew. Chem. Int. Ed.* **2013**, *52*, 3110.

[46] B. Bayatsarmadi, Y. Zheng, Y. Tang, M. Jaroniec, S. Z. Qiao, *Small* **2016**, 12, 3703-3711.

[47] X. Zou, X. Huang, A. Goswami, R. Silva, B. R. Sathe, E. Mikmeková, T. Asefa, *Angew. Chem. Int. Ed.* **2014**, *126*, 4461.

[48] G. L. Tian, M. Q. Zhao, D. Yu, X. Y. Kong, J. Q. Huang, Q. Zhang, F. Wei, *Small* **2014**, *10*, 2251.

[49] Y. Cheng, C. Xu, L. Jia, J. D. Gale, L. Zhang, C. Liu, P. K. Shen, S. P. Jiang, *Appl. Catal. B-Environ.* **2015**, *163*, 96.

[50] G. L. Tian, Q. Zhang, B. Zhang, Y. G. Jin, J. Q. Huang, D. S. Su, F. Wei, *Adv. Funct. Mater.* **2014**, *24*, 5956.

[51] J. Tian, Q. Liu, A. M. Asiri, K. A. Alamry, X. Sun, *ChemSusChem* **2014**, *7*, 2125.

[52] X. Lu, W.-L. Yim, B. H. R. Suryanto, C. Zhao, *J. Am. Chem. Soc.* **2015**, *137*, 2901.

[53] A. M. El‐Sawy, I. M. Mosa, D. Su, C. J. Guild, S. Khalid, R. Joesten, J. F. Rusling, S. L. Suib, *Adv. Energy Mater.* **2016**, 6, 1501966.

[54] X. Yu, M. Zhang, J. Chen, Y. Li, G. Shi, *Adv. Energy Mater.* **2016**, *6*, 1501492.

[55] W. Cui, M. Li, J. Liu, B. Wang, C. Zhang, L. Jiang, Q. Cheng, *ACS Nano* **2014**, *8*, 9511.

[56] R. A. Sidik, A. B. Anderson, N. P. Subramanian, S. P. Kumaraguru, B. N. Popov, *J. Phys. Chem. B* **2006**, *110*, 1787.

[57] L. Zhang, J. Niu, L. Dai, Z. Xia, *Langmuir* **2012**, *28*, 7542.

[58] L. Zhang, Z. Xia, *J. Phys. Chem. C* **2011**, *115*, 11170.

[59] G. Kresse, J. Hafner, *Phys. Rev. B* **1994**, *49*, 14251.

[60] G. Kresse, J. Hafner, *Phys. Rev. B* **1993**, *47*, 558.

[61] G. Kresse, J. Furthmüller, *Phys. Rev. B* **1996**, *54*, 11169.

[62] G. Kresse, J. Furthmüller, *Comp. Mater. Sci.* **1996**, *6*, 15.

[63] J. P. Perdew, K. Burke, M. Ernzerhof, *Phys. Rev. Lett.* **1997**, *78*, 1396.

[64] J. P. Perdew, K. Burke, M. Ernzerhof, *Phys. Rev. Lett.* **1996**, *77*, 3865.

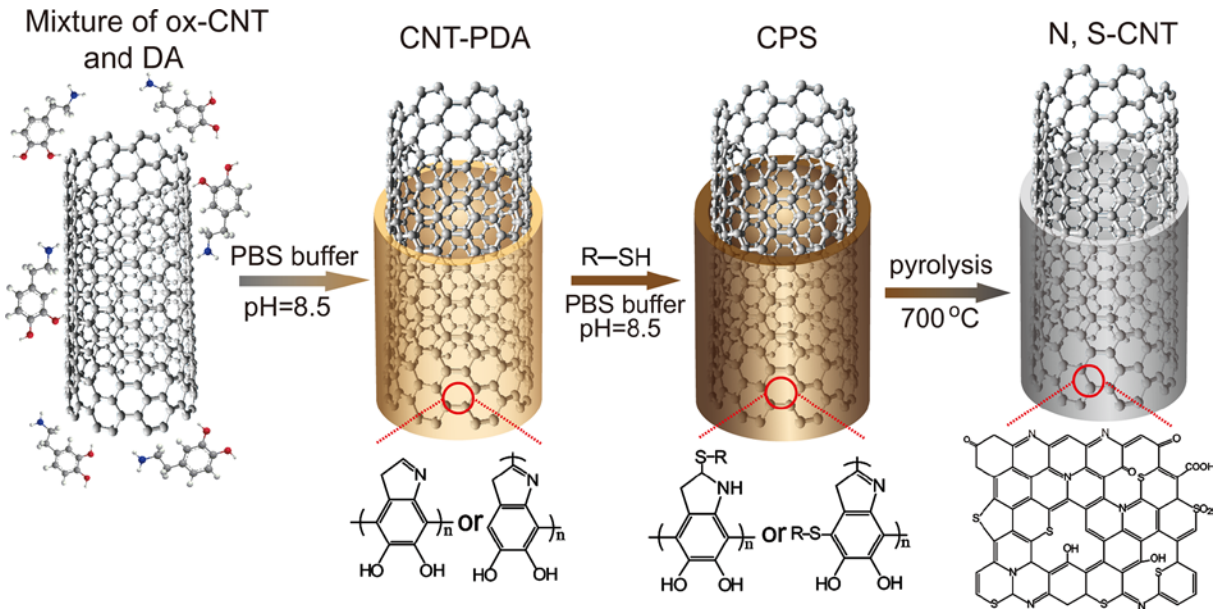

Scheme 1. Fabrication of the N,S-CNT following a two-step "graft-and-pyrolyze" route. The oxidized CNT (ox-CNT) was mixed with dopamine (DA) in PBS buffer to obtain CNT-PDA hybrid. After addition of R-SH, CNT-PDA modified with thiol (CPS) was synthesized, which produced N,S-CNT after pyrolysis. R-SH = 2-mercaptoethanol.

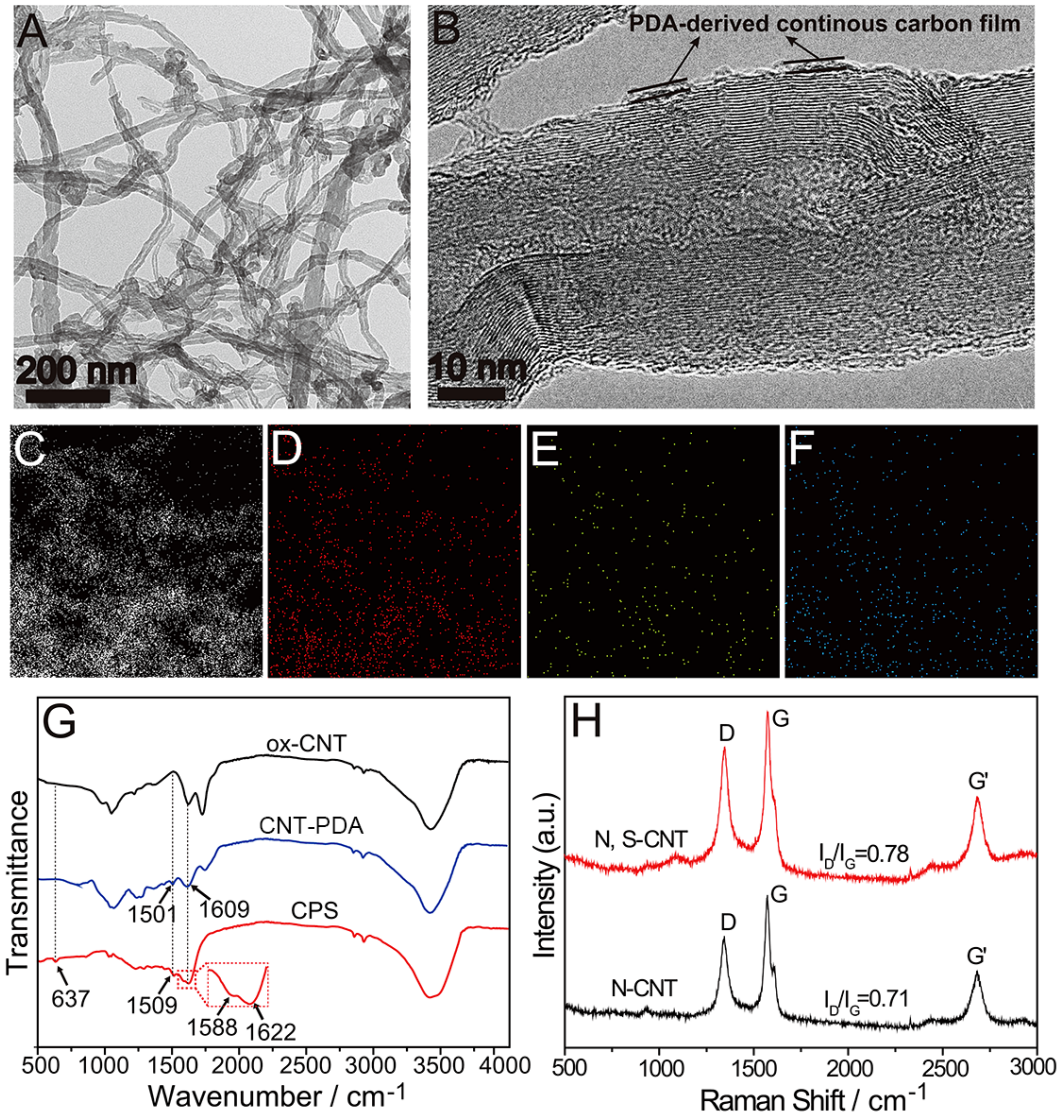

Figure 1. (A) TEM and (B) the magnified TEM images of the N,S-CNT. (C-F) TEM elemental mapping of C, O, N and S in N, S-CN. (G) FTIR spectra of ox-CNT, CNT-PDA and CPS. (H) Raman spectra of N-CNT and N,S-CNT.

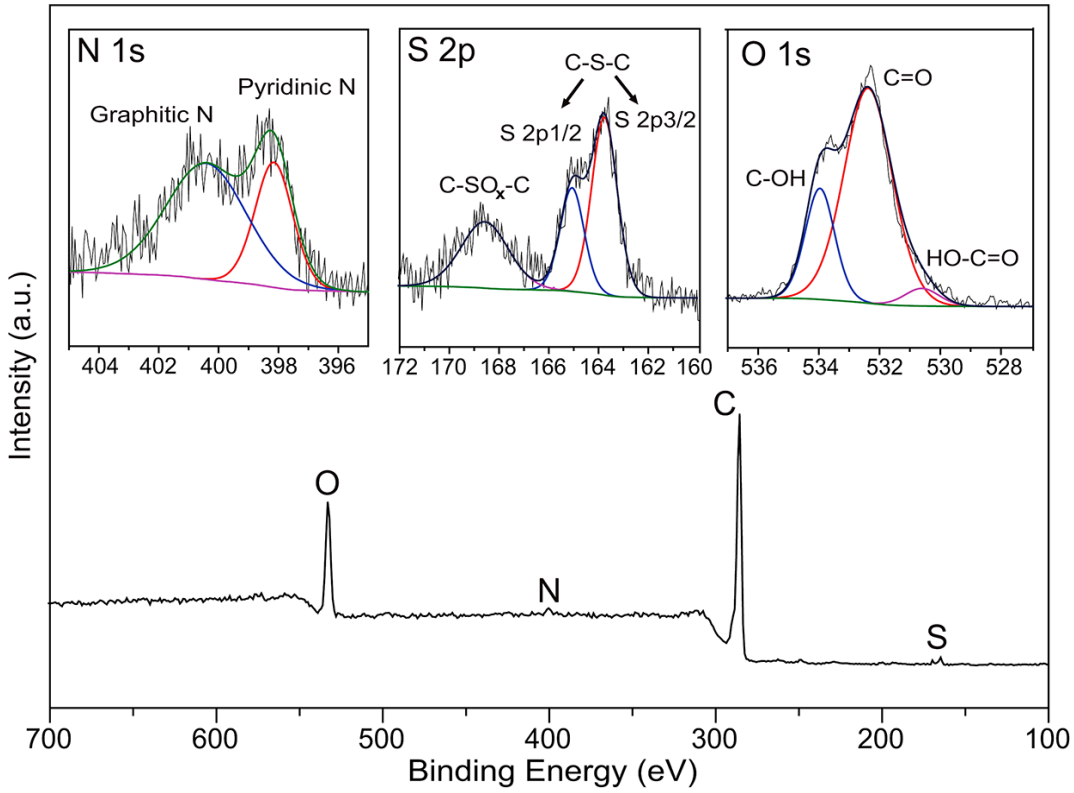

Figure 2. XPS survey and high-resolution spectra of N 1s, S 2p and O 1s in N,S-CNT.

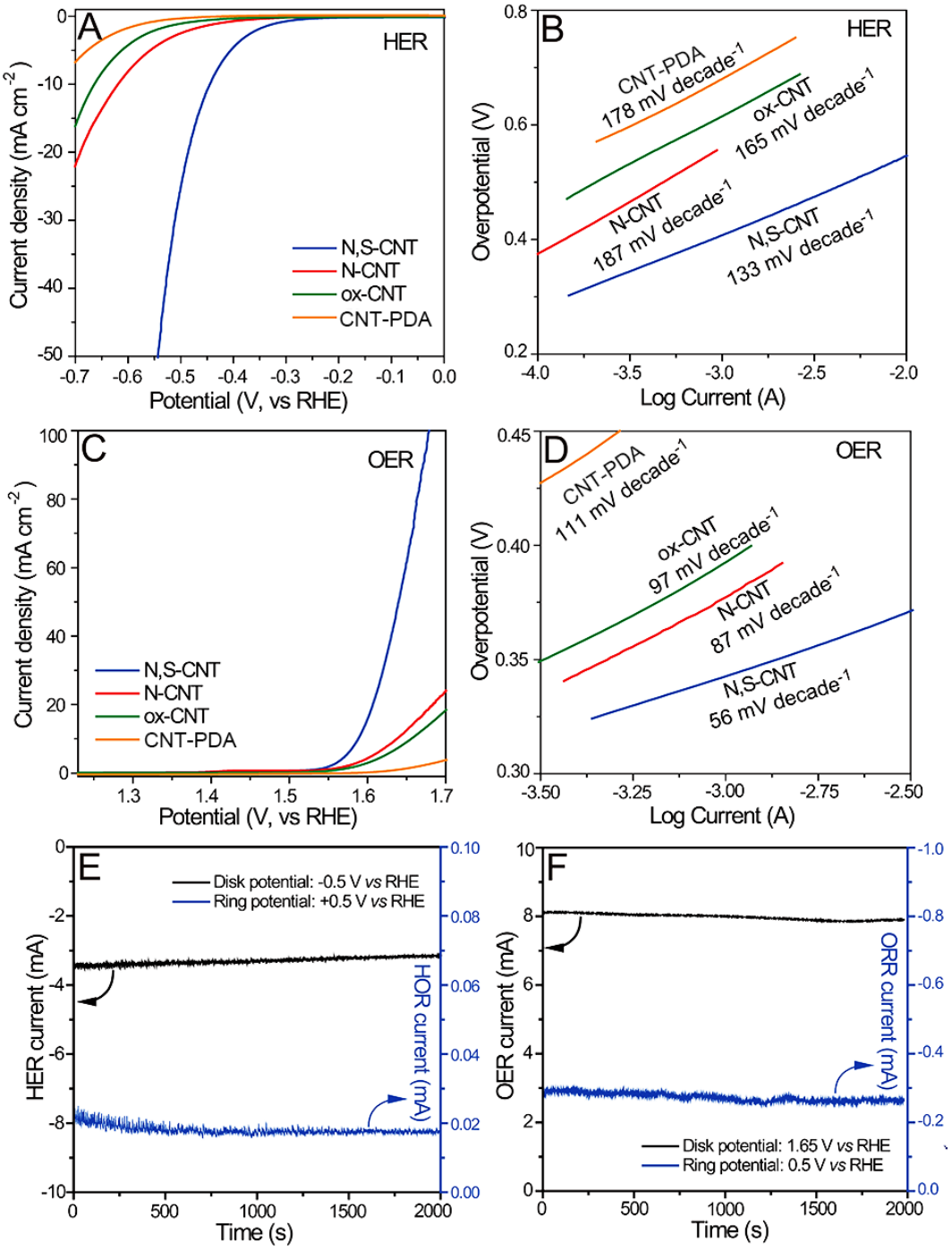

Figure 3. (A) The HER polarization curves and (B) the corresponding Tafel plots of CNT-PDA, ox-CNT, N-CNT and N,S-CNT in 1 M KOH solution. (C) The OER polarization curves and (D) the corresponding Tafel plots of CNT-PDA, ox-CNT, N-CNT and N,S-CNT in 1M KOH solution. (E and F) The current–time chronoamperometric monitor on a RRDE for the generation of H_2 and O_2.

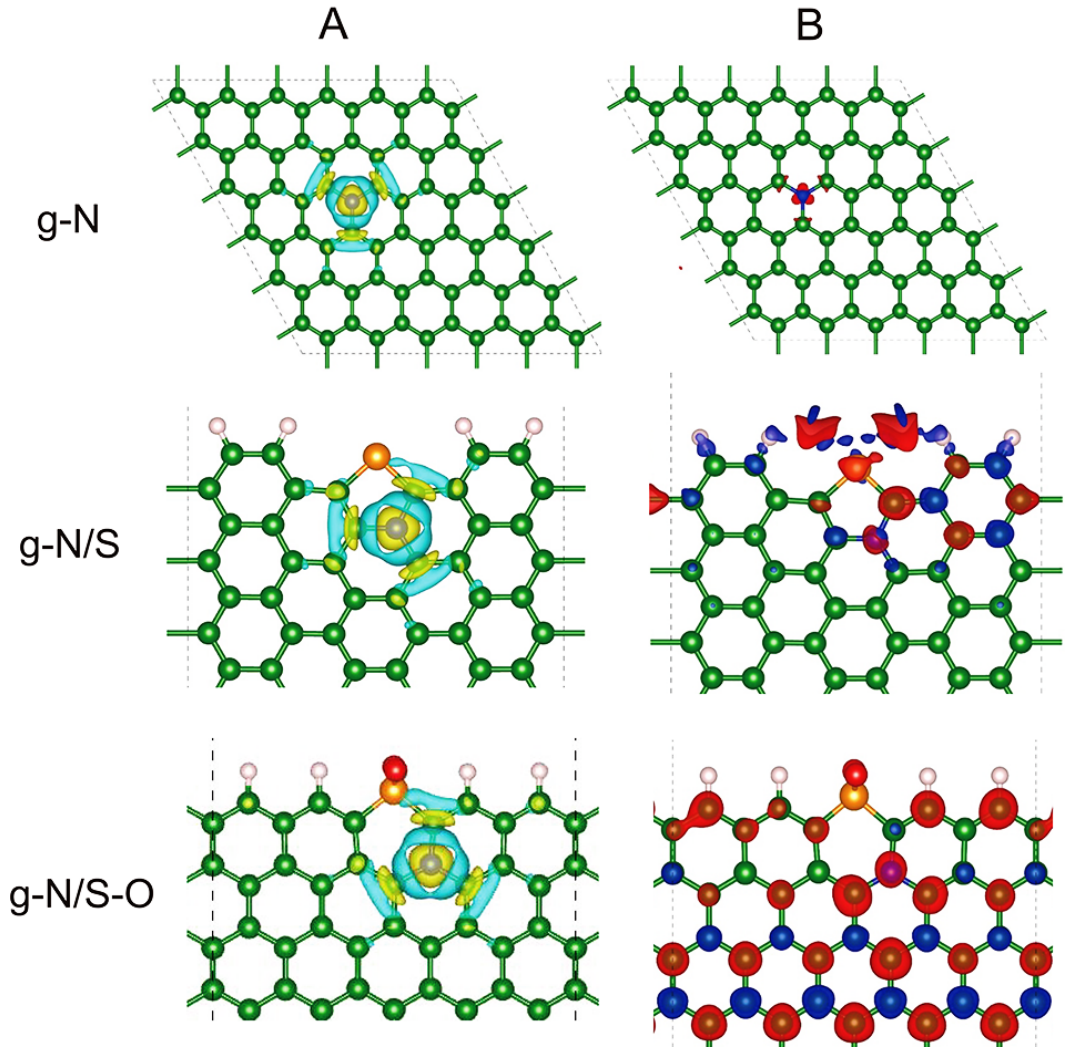

Figure 4. (A) Charge density differences (defined as charge difference led by the incorporation of nitrogen) on various single/double doped models. Isosurface value is 0.02 e/A^3. Yellow and cyan surfaces represent charge accumulation and charge depletion, respectively. (B) Spin density differences (defined as difference between spin up and spin down charge density) on various single/double doped models. Isosurface value for g-N and g-N/S models is 5×10^{-8} e/Å^3 and for g-N/S-O is 1×10^{-3} e/Å^3. Red and blue surfaces represent positive and negative difference, respectively. For the spheres in models (A) and (B), green is carbon, blue is nitrogen, gold is sulphur, red is oxygen and pink is hydrogen. Here we demonstrate the case of g-N co-doped with secondary S heteroatom as which is the major species of nitrogen dopants based on Figure 2 XPS results.

Table of Contents

A metal-free bifunctional HER and OER electroctalyst was designed by the facile polydopamine chemistry to derive N, S-codoping carbon nanotubes with *in-situ*, homogenous and highly efficient S-doping, which exhibited the best HER and OER activity among the reported carbon electrocatalysts. The N,S-codoping carbon nanotube loaded on the carbon cloth was directly used as the anode and cathode for overall water splitting.

Keywords: bifunctional electrocatalysts, nonmetallic codoping, carbon nanotube, polydopamine, water splitting

Konggang Qu, Yao Zheng, Yan Jiao, Prof. Xianxi Zhang, Prof. Sheng Dai,* Prof. Shi-Zhang Qiao*

Polydopamine-Inspired, Dual Heteroatom-Doped Carbon Nanotubes for Highly Efficient Overall Water Splitting

ToC figure